Cronfa - Swansea University Open Access Repository

_____

This is an author produced version of a paper published in:
ACS Macro Letters

_____

Cronfa URL for this paper:
http://cronfa.swan.ac.uk/Record/cronfa45930

_____

Paper:

Cao, S., Abdelmohsen, L., Shao, J., van den Dikkenberg, J., Mastrobattista, E., Williams, D. & van Hest, J. (2018). pH-Induced Transformation of Biodegradable Multilamellar Nanovectors for Enhanced Tumor Penetration. *ACS Macro Letters, 7*(11), 1394-1399.
http://dx.doi.org/10.1021/acsmacrolett.8b00807

http://www.swansea.ac.uk/library/researchsupport/ris-support/

pH-Induced Transformation of Biodegradable Multilamellar Nanovectors for Enhanced Tumor Penetration

Shoupeng Cao,[†] Loai K. E. A. Abdelmohsen,[†] Jingxin Shao,[†] Joep van den Dikkenberg,[§] Enrico Mastrobattista,[§] David S. Williams,*[‡] and Jan C. M. van Hest*[†]

[†]Bio-Organic Chemistry, Institute for Complex Molecular Systems, Eindhoven University of Technology, P.O. Box 513 (STO 3.41), 5600 MB Eindhoven, The Netherlands

[‡]Department of Chemistry, College of Science, Swansea University, Swansea, U.K.

[§]Department of Pharmaceutics, Utrecht Institute for Pharmaceutical Sciences, Utrecht University, Universiteitsweg 99, Utrecht 3584 CG, The Netherlands

S Supporting Information

ABSTRACT: Herein we describe biodegradable nanovectors comprised of block copolymers of poly(ethylene glycol) and poly(trimethylene carbonate) (PEG−PTMC) that change their morphology and surface charge when exposed to tumor environment conditions. Well-defined, drug-loaded nanovectors were prepared via direct hydration using liquid oligo(ethylene glycol) as a dispersant. Systematic introduction of basic imidazole-functional TMC derivatives, through modular polymerization, resulted in polymers that self-assembled in multilamellar nanoparticles (at neutral pH) and that were loaded with hydrophobic drugs. The resultant multilamellar nanovectors demonstrated a significant size reduction and charge reversal at pH ≈ 6.5, which yielded cationic nanovectors that were tailored for tumor penetration. *In vitro* studies using 3D heterospheroids demonstrate that this platform has excellent potential to promote enhanced tumor penetration under physiological conditions.
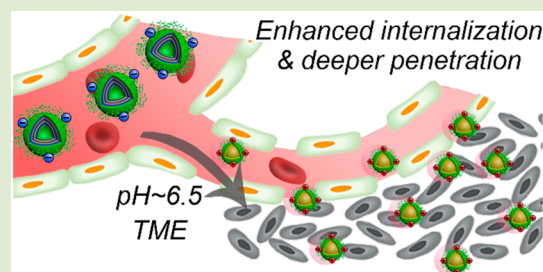
A challenge facing nanomedicine is that the required features of drug nanocarriers for sustained circulation in the body are distinctly different from those necessary for effective drug release at the desired site of action.[1−3] Local application of (noninvasive) physical strategies in order to enhance the therapeutic efficacy by changing particle properties only where required provides one possible solution.[4−6] A higher level of precision is achieved if the physical properties and behavior of nanoparticles are tailored to exploit distinct features already displayed in the microenvironment of the targeted tissue,[7,8] an approach that is receiving an increasing amount of attention. In this respect, the tumor microenvironment (TME) is a highly interesting area to exploit.[9−12] It is well-known that the vasculature, pH, and redox conditions of the TME are considerably different compared to healthy tissue, and many groups have developed strategies to enhance the therapeutic efficacy of their carrier systems by employing, for example, pH-sensitive components.[9] However, in most cases the induced trigger leads to a burst release of the drug and not to changes of the particle features.[13,14] In terms of design criteria, the optimal platform should exist in an uncharged (or partially negative) form with size <100 nm under neutral conditions and, as pH decreases, undergo dynamic reconfiguration into smaller, cationic particles that can effectively penetrate into tumor tissue, delivering cytotoxic payload in a responsive fashion (Figure 1c).[15−17]

Block copolymers (BCPs) are a highly versatile platform for the design and engineering of smart nanosystems,[18−21] and the implementation of BCPs toward anticancer therapy has made significant progress.[22−28] Still, there is much to be gained by exploring the morphology and responsiveness of BCP-based nanosystems to unlock their therapeutic potential.[8,25,28] A significant challenge in the engineering of BCP nanosystems is to maintain functionality while satisfying the fundamental criterion of biocompatibility.[11,29] Few systems exist that demonstrate biodegradability while responding to overtly physiological stimuli (such as pH or redox chemistry).[30−35] Recognizing the strategic importance of the TME, we have undertaken to engineer smart biodegradable nanovectors (NVs) that are capable of undergoing a pH-induced morphology and surface charge switch in order to direct tumor internalization and improve penetration. Key to the success of this strategy is the improved circulation and distribution of nanoparticles with a negative surface charge being physicochemically coupled to the enhanced internalization properties of those with smaller size and positive charge.[7,12] This platform constitutes the first fully biodegradable, stimuli-responsive system that can undergo pH-induced
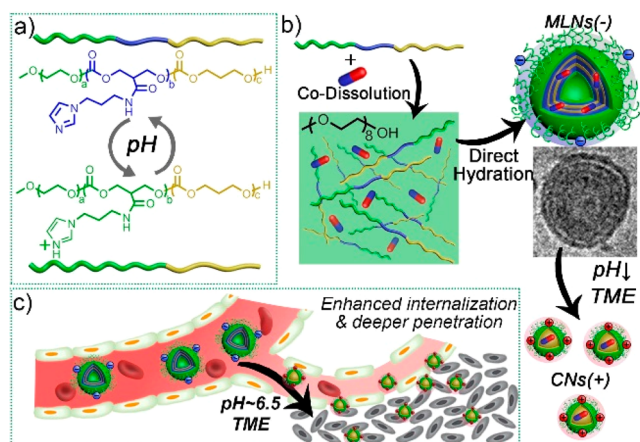
Figure 1. Schematic illustrating (a) the chemical structure of PEG-TMCI-TMC terpolymers and the chemical change that occurs through protonation of imidazole moieties at low pH, (b) fabrication of drug-loaded multilamellar nanovectors (MLNs) via direct hydration and the structural reconfiguration that occurs at low pH into cationic nanovectors (CNs), and (c) the anticipated mode of action of MLNs *in vivo* whereby local pH reduction in the TME leads to enhanced internalization of CNs and tumor penetration.

transformation into nanoparticles that demonstrate enhanced tumor penetration.

Recently, we have presented an approach toward the fabrication of both drug-loaded NVs and enzyme-loaded nanoreactors, comprising biodegradable copolymers based on poly(ethylene glycol)-*block*-poly(trimethylene carbonate) (PEG−PTMC) and utilizing direct hydration as a facile, biocompatible, fabrication process.[36,37] PEG−PTMC copolymers provide the necessary structural versatility necessary to engineer particles that are capable of undergoing dynamic transformations.[29,38−40]

pH-responsive functionality was introduced into PEG-PTMC copolymers using carbonate monomers with a basic imidazole moiety (TMCI, $pK_a \approx 6.5$) to create terpolymeric chains that could induce dynamic reconfiguration under conditions similar to the TME (Figure 1a). Using the direct hydration methodology, self-assembly of PEG−PTMC copolymers comprising TMCI was assessed by systematically varying the block configuration in order to identify the nexus between size, stability, and dynamicity (Figure 1b).

PEG−PTMC copolymers with well-defined sequences were synthesized via the sequential ring-opening polymerization of TMC and TMC-OPhF5 monomers, with pH-responsive imidazole moieties introduced by postpolymerization (Scheme S1).[34,41−43] In terms of copolymer design, we evaluated the effect of TMCI upon the self-assembly and pH-induced reconfiguration of particles to identify the optimal composition that would yield the desired design criteria. As PEG$_{22}$-PTMC$_{30}$ BCPs were known to yield well-defined micelles, we used this as the basis to prepare terpolymers where TMCI occupied either the terminal or intermediate position (Table S4). Assessing the terminal PEG-TMC-TMCI copolymers demonstrated that shorter PTMC blocks (DP = 23 vs 30) did not display a pronounced size change upon acidic pH incubation, and longer PTMCI blocks (DP = 10 vs 7) resulted in visible aggregations (Figure S23). The size change behavior of PEG-TMC-TMCI BCPs was not optimal at pH 6.5, with 2 h incubation yielding around 60 nm nanoparticles and no significant size decrease after prolonged incubation (Figure

S24a). Introducing PTMCI in the intermediate terpolymer position was a more effective strategy. PEG-TMCI-TMC copolymers also showed a pH-induced size change (130−140 vs 43 nm, at pH 7.4 and 6.5, respectively). We observed a marked advantage with PEG$_{22}$-TMCI$_7$-TMC$_{30}$, which underwent effective reconfiguration in 2 h at pH 6.5 toward nanoparticles of 40 nm, possibly because of improved access to protonation (compared to PEG-TMC$_{30}$-TMCI$_7$) and reduced hydrophilic repulsion (compared to PEG-TMCI$_{10}$-TMC$_{30}$) (Figure S25 and S26).[31,40] To highlight the importance of structural control in directing this pH-responsive behavior, the random copolymer of TMC and TMCI was prepared. PEG-(TMC-*r*-TMCI) BCPs underwent self-assembly under neutral conditions but disassembled at low pH, with only large (>600 nm), poorly defined particles evident by dynamic light scattering (DLS) (Figure S27). Nonresponsive TMC-based polymersomes did not show significant size or zeta potential change when incubated in an acidic buffer (Figure S28).[37]

Having identified PEG$_{22}$-TMCI$_7$-TMC$_{30}$ as an excellent candidate for the formation of a pH-responsive nanosystem, its self-assembly was studied in greater detail. Under neutral conditions, cryo-TEM images showed that the terpolymer underwent self-assembly into multilamellar nanovectors (MLNs, Figure 2a/S30), which is consistent with DLS data. At low pH, MLNs underwent reorganization into cationic nanovectors (CNs) with micellar morphology (Figure 2b/S32). Scanning electron microscopy (SEM) further confirmed the size switch behavior of MLNs (Figure S33). MLN to CN
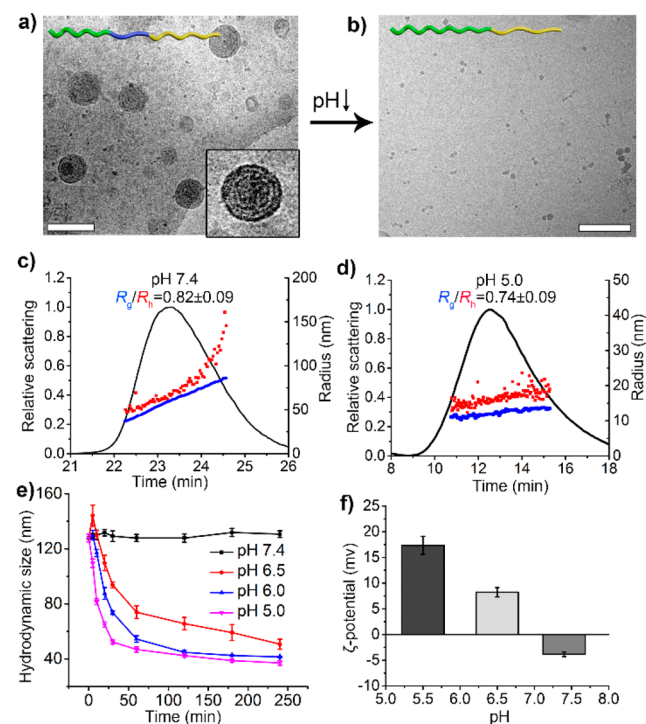

Figure 2. pH-induced transformation of multilamellar nanovectors (MLNs) into cationic nanovectors (CNs) comprising PEG$_{22}$-TMCI$_7$-TMC$_{30}$ terpolymers. TEM images of (a) MLNs and (b) CNs after reduction in pH (scale bars = 100 nm). AF4 fractogram (scattering profile in black) of (c) MLNs at pH 7.4 and (d) after transformation to CNs at pH 5 comparing the radius of gyration (R_g, blue) to the hydrodynamic radius (R_h, red). (e) Real-time monitoring of the pH-induced transformation of MLNs by DLS. (f) Zeta-potential measurements of MLNs/CNs at varying pH.

transformation is driven by the flexibility of the TMC block and imidazole protonation, which increased interchain repulsion and facilitated micellization,[30,40] with the resulting micelles having increasingly cationic character as determined by zeta-potential measurements (Figure 2f). For quantitative insight into the particle morphology, we employed asymmetric flow field−flow fractionation (AF4) coupled with multiangle light scattering (MALS) and DLS. Consistent with cryo-TEM data, MLNs possessed an average hydrodynamic radius (R_h) of 73.1 nm with particles ranging from 47.2 to 117.4 nm. Comparing this to the radius of gyration (R_g) yielded a shape factor (R_g/R_h) of 0.82, consistent with filled spheres (Figure 2c/S34a). CNs displayed a much more uniform size profile, with R_h values between 12.8 and 23.4 nm (average 16.6 nm); moreover, the shape factor 0.74 indicated a micellar morphology (Figure 2d/S34b). The critical aggregation concentration (CAC) of MLNs/CNs was determined using 1-anilino-8-naphthalenesulfonate (ANS) assay. Before and after protonation, CAC values were measured at ca. 0.017 (2.7 μM) and 0.026 mg/mL (4.2 μM), respectively (Figure S36).

We next monitored the performance of MLNs to undergo an efficient size switch under increasingly acidic conditions. A significant decrease in particle size was observed within 60 min at pH values of 5, 6, and 6.5, with no evidence of larger particles after 4 h (Figure 2e). After only 30 min at pH 6.5, both morphologies were evident by cryo-TEM as the size switch from MLNs to CNs was ongoing (Figure S31). AF4 data for MLNs incubated at pH 6.5 for 2 h indicated that the transformation to CNs was complete, with values of R_h comparable to those at pH 5 (Figure S35).

In vitro performance of MLNs was studied using HepG2 cells to assess the functional impact of the pH-induced transformation. Chlorin e6 (Ce6)-labeled MLNs (Scheme S1) were utilized for fluorescence visualization of particle uptake; the presence of 2 wt % PEG-PTMC-Ce6 did not affect the responsive nature of the particles (Figure S29a). After incubation of the cells with MLNs at pH 6.5, it was clear from microscopy (Figure 3a/S40) and flow cytometry (Figure 3b/S41) that CNs demonstrated enhanced cellular uptake as compared to MLNs. Interestingly, this distinct behavior was already observed after 30 min, which increased further after an hour as the pH-induced transformation progressed (Figure S41). Nonresponsive control polymersomes did not show any change in cellular uptake between normal physiological pH and acidic conditions (Figure S42). Furthermore, we confirmed that under these conditions (pH 7.4/6.5) little toxicity was observed up to [copolymer] = 0.2 mg/mL ($\approx$70%, Figure S38).

Next, we assessed the capacity of this pH-responsive platform to deliver cytotoxic cargo and to determine what effect structural reconfiguration would have on this process. Using a hydrophobic cisplatin prodrug (Figure S39a) we prepared MLNs with 9.3 wt % loading with 93% efficiency.[44] At lower pH drug was released from CNs more rapidly (ca. 75 and 90% released after 24 h at pH 6.5 and 5.5, respectively) as compared to MLNs at neutral pH (Figure S39b). Cytotoxicity was tested against both HeLa and HepG2 cell lines. As with HepG2 cells, little background toxicity was observed for the unloaded particles at [copolymer] < 0.2 mg/mL, both at neutral pH and pH 6.5 (Figure S38). Prodrug cytotoxicity was enhanced through encapsulation in MLNs against HeLa and HepG2 cells (HeLa, IC$_{50}$ free prodrug: 16.0 μM, IC$_{50}$ prodrug
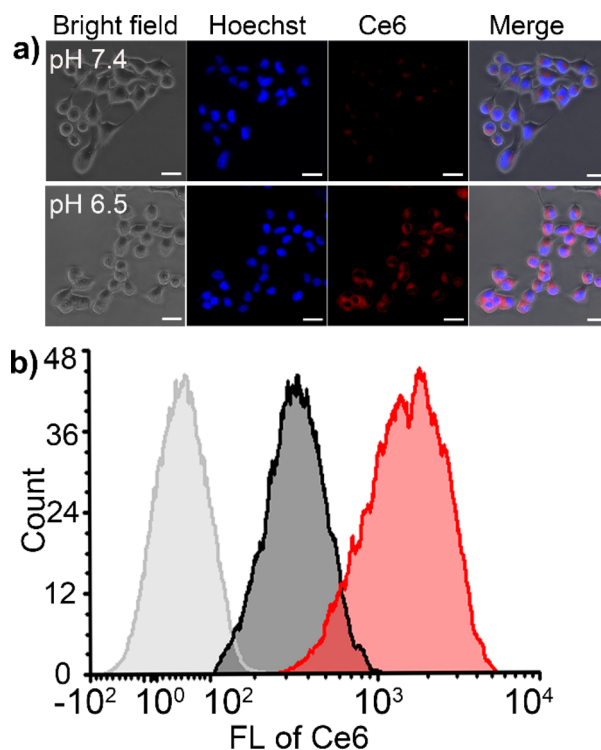

Figure 3. MLN performance *in vitro*. (a) Fluorescent images of HepG2 cells treated with Ce6-labeled MLNs for 2 h at pH 7.4 and 6.5 (scale bar = 20 μm). (b) Flow cytometry results for uptake into HepG2 cells at pH 7.4 (gray) and 6.5 (red) compared to control cells (light gray).

loaded: 3.3 μM; HepG2, IC$_{50}$ free prodrug: 10.3 μM, IC$_{50}$ prodrug loaded: 1.8 μM, Figure 4a/b). At pH 6.5 this effect was more pronounced (HeLa, IC$_{50}$ prodrug loaded: 1.5 μM; HepG2, IC$_{50}$ prodrug loaded: 0.7 μM), demonstrating the formation of CNs did not diminish the therapeutic performance of encapsulated cargo despite the pH-induced structural reconfiguration.
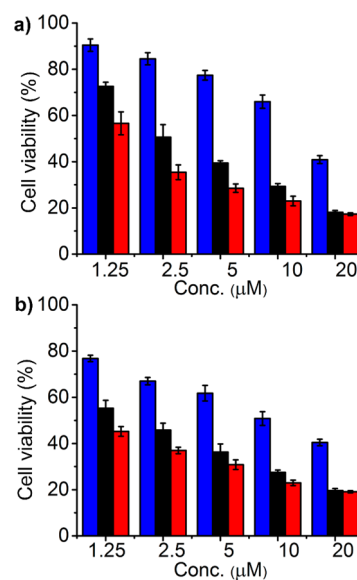

Figure 4. MLN performance *in vitro*. Cell viability of (a) HeLa and (b) HepG2 cells after treatment with free cisplatin prodrug (blue) and drug-loaded MLNs at pH 7.4 (black) and 6.5 (red).

Lastly, to determine whether this behavior would translate to a more biologically relevant platform we studied multicellular spheroids (MCSs) as tumor models *in vitro*.[35,45] Using confocal laser scanning microscopy (CLSM) stack imaging it was apparent that after 2 h MLNs (at pH 7.4) were principally located on the periphery of MCSs with a penetration depth of 40−60 μm, whereas CNs (at pH 6.5) showed enhanced penetration (Figure S43). After 18 h incubation, although MLNs (at pH 7.4) did not show a significant change in the penetration profile, CNs (at pH 6.5) showed significantly enhanced penetration to depths of 180 μm (Figure 5a/b, S44).
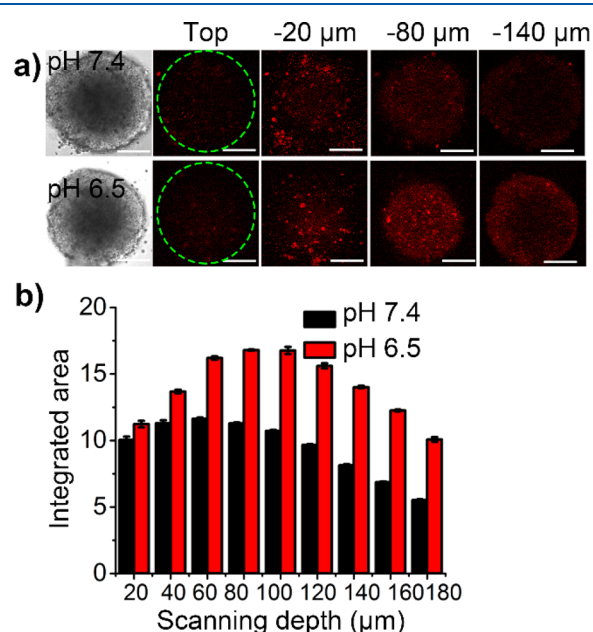

Figure 5. MLN performance *in vitro*. (a) Fluorescent images following penetration into 3D MCSs at pH 7.4 and 6.5 (scale bar = 200 μm). (b) Quantification of fluorescent data in (c) after 18 h of treatment.

Similar results were obtained with penetration studies on heterospheroids, comprising a mixture of HepG2 cells and fibroblast 3T3 cells (1:5) (Figure S45).[45] As a further control, we confirmed that nonresponsive polymersomes did not undergo any increase in penetration at lower pH (Figure S46/S47). These results suggest that the pH-induced transformation of MLNs into CNs can enhance tumor penetration under physiological conditions and that this pH-responsive MLN/CN system can be an effective strategy for the treatment of cancer.

In summary, we present biodegradable BCP assemblies with pH-responsive behavior such that, at low pH, a morphology switch occurs resulting in the formation of highly penetrating cationic nanovectors. This is achieved by implementing imidazole-modified domains ($pK_a \approx 6.5$) in the flexible polycarbonates, which induce the alteration of amphiphilicity and charge under pH conditions alike to the tumor microenvironment. The dynamic morphology and surface charge modulation of these biodegradable nanovectors provide desirable physicochemical features that could enable targeted delivery and deeper penetration in tumor tissue.

ASSOCIATED CONTENT

Supporting Information

The Supporting Information is available free of charge on the ACS Publications website at DOI: 10.1021/acsmacrolett.8b00807.

Included are details of materials, methods, synthesis, and other supporting data utilized in this work (PDF)

AUTHOR INFORMATION

Corresponding Authors

*Jan C. M. van Hest (j.c.m.v.hest@tue.nl).
*David S. Williams (d.s.williams@swansea.ac.uk).

ORCID

Loai K. E. A. Abdelmohsen: 0000-0002-0094-1893
Enrico Mastrobattista: 0000-0002-6745-2015
David S. Williams: 0000-0002-8209-6899
Jan C. M. van Hest: 0000-0001-7973-2404

Notes

The authors declare no competing financial interest.

REFERENCES

(1) Peer, D.; Karp, J. M.; Hong, S.; Farokhzad, O. C.; Margalit, R.; Langer, R. Nanocarriers as an Emerging Platform for Cancer Therapy. *Nat. Nanotechnol.* 2007, 2, 751.

(2) Sanhai, W. R.; Sakamoto, J. H.; Canady, R.; Ferrari, M. Seven Challenges for Nanomedicine. *Nat. Nanotechnol.* 2008, 3, 242−244.

(3) Davis, M. E.; Chen, Z.; Shin, D. M. Nanoparticle Therapeutics: An Emerging Treatment Modality for Cancer. *Nat. Rev. Drug Discovery* 2008, 7, 771−782.

(4) Petros, R. A.; DeSimone, J. M. Strategies in the Design of Nanoparticles for Therapeutic Applications. *Nat. Rev. Drug Discovery* 2010, 9, 615.

(5) Torchilin, V. P. Multifunctional, Stimuli-Sensitive Nanoparticulate Systems for Drug Delivery. *Nat. Rev. Drug Discovery* 2014, 13, 813.

(6) Blanco, E.; Shen, H.; Ferrari, M. Principles of Nanoparticle Design for Overcoming Biological Barriers To Drug Delivery. *Nat. Biotechnol.* 2015, 33, 941−951.

(7) Cheng, R.; Meng, F.; Deng, C.; Zhong, Z. Bioresponsive Polymeric Nanotherapeutics for Targeted Cancer Chemotherapy. *Nano Today* 2015, 10, 656−670.

(8) Mura, S.; Nicolas, J.; Couvreur, P. Stimuli-Responsive Nanocarriers for Drug Delivery. *Nat. Mater.* 2013, 12, 991.

(9) Mo, R.; Gu, Z. Tumor Microenvironment and Intracellular Signal-Activated Nanomaterials for Anticancer Drug Delivery. *Mater. Today* 2016, 19, 274−283.

(10) Wang, Y.; Zhou, K.; Huang, G.; Hensley, C.; Huang, X.; Ma, X.; Zhao, T.; Sumer, B. D.; DeBerardinis, R. J.; Gao, J. A Nanoparticle-Based Strategy for the Imaging of a Broad Range of

Tumours by Nonlinear Amplification of Microenvironment Signals. *Nat. Mater.* **2014**, *13*, 204.

(11) Dai, Y.; Xu, C.; Sun, X.; Chen, X. Nanoparticle Design Strategies for Enhanced Anticancer Therapy by Exploiting the Tumour Microenvironment. *Chem. Soc. Rev.* **2017**, *46*, 3830−3852.

(12) Feng, L.; Dong, Z.; Tao, D.; Zhang, Y.; Liu, Z. The Acidic Tumor Microenvironment: A Target for Smart Cancer Nano-Theranostics. *Natl. Sci. Rev.* **2018**, *5*, 269−286.

(13) Yang, K.; Chang, Y.; Wen, J.; Lu, Y.; Pei, Y.; Cao, S.; Wang, F.; Pei, Z. Supramolecular Vesicles Based on Complex of Trp-Modified Pillar[5]arene and Galactose Derivative for Synergistic and Targeted Drug Delivery. *Chem. Mater.* **2016**, *28*, 1990−1993.

(14) Cao, S.; Pei, Z.; Xu, Y.; Pei, Y. Glyco-Nanovesicles with Activatable Near-Infrared Probes for Real-Time Monitoring of Drug Release and Targeted Delivery. *Chem. Mater.* **2016**, *28*, 4501−4506.

(15) Wang, J.; Mao, W.; Lock, L. L.; Tang, J.; Sui, M.; Sun, W.; Cui, H.; Xu, D.; Shen, Y. The Role of Micelle Size in Tumor Accumulation, Penetration, and Treatment. *ACS Nano* **2015**, *9*, 7195−7206.

(16) Sun, Q.; Sun, X.; Ma, X.; Zhou, Z.; Jin, E.; Zhang, B.; Shen, Y.; Van Kirk, E. A.; Murdoch, W. J.; Lott, J. R.; Lodge, T. P.; Radosz, M.; Zhao, Y. Integration of Nanoassembly Functions for an Effective Delivery Cascade for Cancer Drugs. *Adv. Mater.* **2014**, *26*, 7615−7621.

(17) Tang, L.; Yang, X.; Yin, Q.; Cai, K.; Wang, H.; Chaudhury, I.; Yao, C.; Zhou, Q.; Kwon, M.; Hartman, J. A.; Dobrucki, I. T.; Dobrucki, L. W.; Borst, L. B.; Lezmi, S.; Helferich, W. G.; Ferguson, A. L.; Fan, T. M.; Cheng, J. Investigating the Optimal Size of Anticancer Nanomedicine. *Proc. Natl. Acad. Sci. U. S. A.* **2014**, *111*, 15344−15349.

(18) Mai, Y.; Eisenberg, A. Self-Assembly of Block Copolymers. *Chem. Soc. Rev.* **2012**, *41*, 5969−5985.

(19) van Dongen, S. F. M.; de Hoog, H.-P. M.; Peters, R. J. R. W.; Nallani, M.; Nolte, R. J. M.; van Hest, J. C. M. Biohybrid Polymer Capsules. *Chem. Rev.* **2009**, *109*, 6212−6274.

(20) Wiradharma, N.; Zhang, Y.; Venkataraman, S.; Hedrick, J. L.; Yang, Y. Y. Self-Assembled Polymer Nanostructures for Delivery of Anticancer Therapeutics. *Nano Today* **2009**, *4*, 302−317.

(21) Kim, S. H.; Nederberg, F.; Jakobs, R.; Tan, J. P. K.; Fukushima, K.; Nelson, A.; Meijer, E. W.; Yang, Y. Y.; Hedrick, J. L. A Supramolecularly Assisted Transformation of Block-Copolymer Micelles into Nanotubes. *Angew. Chem., Int. Ed.* **2009**, *48*, 4508−4512.

(22) Shi, Y.; van der Meel, R.; Theek, B.; Oude Blenke, E.; Pieters, E. H. E.; Fens, M. H. A. M.; Ehling, J.; Schiffelers, R. M.; Storm, G.; van Nostrum, C. F.; Lammers, T.; Hennink, W. E. Complete Regression of Xenograft Tumors upon Targeted Delivery of Paclitaxel via Π−Π Stacking Stabilized Polymeric Micelles. *ACS Nano* **2015**, *9*, 3740−3752.

(23) Wang, S.; Huang, P.; Chen, X. Hierarchical Targeting Strategy for Enhanced Tumor Tissue Accumulation/Retention and Cellular Internalization. *Adv. Mater.* **2016**, *28*, 7340−7364.

(24) Xu, X.; Wu, J.; Liu, Y.; Yu, M.; Zhao, L.; Zhu, X.; Bhasin, S.; Li, Q.; Ha, E.; Shi, J.; Farokhzad Omid, C. Ultra-pH-Responsive and Tumor-Penetrating Nanoplatform for Targeted siRNA Delivery with Robust Anti-Cancer Efficacy. *Angew. Chem., Int. Ed.* **2016**, *55*, 7091−7094.

(25) Fukushima, K.; Tan, J. P. K.; Korevaar, P. A.; Yang, Y. Y.; Pitera, J.; Nelson, A.; Maune, H.; Coady, D. J.; Frommer, J. E.; Engler, A. C.; Huang, Y.; Xu, K.; Ji, Z.; Qiao, Y.; Fan, W.; Li, L.; Wiradharma, N.; Meijer, E. W.; Hedrick, J. L. Broad-Spectrum Antimicrobial Supramolecular Assemblies with Distinctive Size and Shape. *ACS Nano* **2012**, *6*, 9191−9199.

(26) Abdelmohsen, L. K. E. A.; Williams, D. S.; Pille, J.; Ozel, S. G.; Rikken, R. S. M.; Wilson, D. A.; van Hest, J. C. M. Formation of Well-Defined, Functional Nanotubes via Osmotically Induced Shape Transformation of Biodegradable Polymersomes. *J. Am. Chem. Soc.* **2016**, *138*, 9353−9356.

(27) Pijpers, I. A. B.; Abdelmohsen, L. K. E. A.; Williams, D. S.; van Hest, J. C. M. Morphology Under Control: Engineering Biodegradable Stomatocytes. *ACS Macro Lett.* **2017**, *6*, 1217−1222.

(28) Williams, D. S.; Pijpers, I. A. B.; Ridolfo, R.; van Hest, J. C. M. Controlling the Morphology of Copolymeric Vectors for Next Generation Nanomedicine. *J. Controlled Release* **2017**, *259*, 29−39.

(29) Deng, C.; Jiang, Y.; Cheng, R.; Meng, F.; Zhong, Z. Biodegradable Polymeric Micelles for Targeted and Controlled Anticancer Drug Delivery: Promises, Progress and Prospects. *Nano Today* **2012**, *7*, 467−480.

(30) Yan, Q.; Zhao, Y. Polymeric Microtubules That Breathe: CO2-Driven Polymer Controlled-Self-Assembly and Shape Transformation. *Angew. Chem., Int. Ed.* **2013**, *52*, 9948−9951.

(31) Yan, Q.; Zhao, Y. CO2-Stimulated Diversiform Deformations of Polymer Assemblies. *J. Am. Chem. Soc.* **2013**, *135*, 16300−16303.

(32) Che, H.; Cao, S.; van Hest, J. C. M. Feedback-Induced Temporal Control of "Breathing" Polymersomes To Create Self-Adaptive Nanoreactors. *J. Am. Chem. Soc.* **2018**, *140*, 5356−5359.

(33) Qi, W.; Zhang, Y.; Wang, J.; Tao, G.; Wu, L.; Kochovski, Z.; Gao, H.; Chen, G.; Jiang, M. Deprotection-Induced Morphology Transition and Immunoactivation of Glycovesicles: A Strategy of Smart Delivery Polymersomes. *J. Am. Chem. Soc.* **2018**, *140*, 8851−8857.

(34) Chan, J. M. W.; Tan, J. P. K.; Engler, A. C.; Ke, X.; Gao, S.; Yang, C.; Sardon, H.; Yang, Y. Y.; Hedrick, J. L. Organocatalytic Anticancer Drug Loading of Degradable Polymeric Mixed Micelles via a Biomimetic Mechanism. *Macromolecules* **2016**, *49*, 2013−2021.

(35) Chen, J.; Ding, J.; Wang, Y.; Cheng, J.; Ji, S.; Zhuang, X.; Chen, X. Sequentially Responsive Shell-Stacked Nanoparticles for Deep Penetration into Solid Tumors. *Adv. Mater.* **2017**, *29*, 1701170.

(36) Ridolfo, R.; Ede, B. C.; Diamanti, P.; White, P. B.; Perriman, A. W.; van Hest, J. C. M.; Blair, A.; Williams, D. S. Biodegradable, Drug-Loaded Nanovectors via Direct Hydration as a New Platform for Cancer Therapeutics. *Small* **2018**, *14*, 1703774.

(37) van Oppen, L. M. P. E.; Abdelmohsen, L. K. E. A.; van Emst-de Vries, S. E.; Welzen, P. L. W.; Wilson, D. A.; Smeitink, J. A. M.; Koopman, W. J. H.; Brock, R.; Willems, P. H. G. M.; Williams, D. S.; van Hest, J. C. M. Biodegradable Synthetic Organelles Demonstrate ROS Shielding in Human-Complex-I-Deficient Fibroblasts. *ACS Cent. Sci.* **2018**, *4*, 917−928.

(38) Fukushima, K. Poly(trimethylene carbonate)-Based Polymers Engineered for Biodegradable Functional Biomaterials. *Biomater. Sci.* **2016**, *4*, 9−24.

(39) Chen, W.; Meng, F.; Cheng, R.; Deng, C.; Feijen, J.; Zhong, Z. Advanced Drug and Gene Delivery Systems Based on Functional Biodegradable Polycarbonates and Copolymers. *J. Controlled Release* **2014**, *190*, 398−414.

(40) Nederberg, F.; Zhang, Y.; Tan, J. P. K.; Xu, K.; Wang, H.; Yang, C.; Gao, S.; Guo, X. D.; Fukushima, K.; Li, L.; Hedrick, J. L.; Yang, Y.-Y. Biodegradable Nanostructures with Selective Lysis of Microbial Membranes. *Nat. Chem.* **2011**, *3*, 409.

(41) Kamber, N. E.; Jeong, W.; Waymouth, R. M.; Pratt, R. C.; Lohmeijer, B. G. G.; Hedrick, J. L. Organocatalytic Ring-Opening Polymerization. *Chem. Rev.* **2007**, *107*, 5813−5840.

(42) Sanders, D. P.; Fukushima, K.; Coady, D. J.; Nelson, A.; Fujiwara, M.; Yasumoto, M.; Hedrick, J. L. A Simple and Efficient Synthesis of Functionalized Cyclic Carbonate Monomers Using a Versatile Pentafluorophenyl Ester Intermediate. *J. Am. Chem. Soc.* **2010**, *132*, 14724−14726.

(43) Chan, J. M. W.; Ke, X.; Sardon, H.; Engler, A. C.; Yang, Y. Y.; Hedrick, J. L. Chemically Modifiable N-heterocycle-Functionalized Polycarbonates as a Platform for Diverse Smart Biomimetic Nanomaterials. *Chem. Sci.* **2014**, *5*, 3294−3300.

(44) Dhar, S.; Gu, F. X.; Langer, R.; Farokhzad, O. C.; Lippard, S. J. Targeted Delivery of Cisplatin to Prostate Cancer Cells by Aptamer Functionalized Pt(IV) Prodrug-PLGA−PEG Nanoparticles. *Proc. Natl. Acad. Sci. U. S. A.* **2008**, *105*, 17356−17361.

(45) Priwitaningrum, D. L.; Blondé, J.-B. G.; Sridhar, A.; van Baarlen, J.; Hennink, W. E.; Storm, G.; Le Gac, S.; Prakash, J. Tumor

Stroma-Containing 3D Spheroid Arrays: A Tool to Study Nano-particle Penetration. *J. Controlled Release* **2016**, *244*, 257−268.